From partial to complete neutralization of 2,5-dihydroxyterephthalic acid in the Li–Na system: crystal chemistry and electrochemical behavior of Na 2 Li 2 C 8 H 2 O 6 vs. Li

Eric Quarez, Alia Jouhara, Stéphane Grolleau, Franck Dolhem, Nicolas Dupre, Philippe Poizot

From partial to complete neutralization of 2,5-dihydroxyterephthalic acid in the Li–Na system: crystal chemistry and electrochemical behavior of $Na_2Li_2C_8H_2O_6$ vs. Li

Éric Quarez, *[a] Alia Jouhara,[a] Stéphane Grolleau,[a] Franck Dolhem, [b] Nicolas Dupré[a] and Philippe Poizot

The 2,5-dihydroxyterephthalic acid (H_4-p-DHT) is of special interest in the field of materials science because of the two symmetric sets of oxygen donor functional groups (i.e., β-hydroxy acid moieties). In its partially (–2H) or totally (–4H) deprotonated form, it is an efficient organic ligand making the synthesis of numerous coordination polymers possible. In addition, it exhibits dual redox-active properties, which make it very interesting as electrode material when combined with alkali and alkaline-earth elements. Herein, we report on a specific study on alkali salts obtained from partial to complete neutralization of 2,5-dihydroxyterephthalic acid in the Li–Na system, which notably enable us to prepare the mixed phase Na_2IJLi_2)-p-DHT ($Na_2Li_2C_8H_2O_6$) and to test it electrochemically vs. Li. Depending on the experimental conditions, two Li-polymorphs and one Na compound, containing H_2-p-DHT^{2-} ligands with deprotonated carboxylic groups, were obtained, namely, M_2IJH_2)-p-DHT(H_2O)$_4$ M = Li (1, 2) and Na (3) as well as the first mixed alkali metal compound, i.e. Na_2IJLi_2)-p-DHT(H_2O)$_8$ (4). The single crystal structure analyses showed that all compounds display various inorganic motifs with discrete LiO_4 tetrahedra (1, 2), Li_2O_6 dimers of edge-sharing LiO_4 tetrahedra (2), $^1_\infty[NaO_4]^{-7}$ 1-D chains of edge-sharing NaO_6 octahedra (3) and $[Li_2Na_2O_{14}]^{24-}$ clusters of LiO_4 tetrahedra and NaO_6 octahedra (4). The electrochemical assessment of the anhydrous Na_2IJLi_2)-p-DHT compound measured in Li half-cell revealed however poor performances compared to Li_4-p-DHT ($Li_4C_8H_2O_6$) due to cationic disorder of the two alkali ions in the crystal structure giving rise to the progressive conversion of the pristine phase to Li_4-p-DHT upon cycling.

1. Introduction

The discovery of metal–organic frameworks (MOFs) or coordination polymers (CPs) at the end of the eighties enabled the development of a myriad of new functional materials giving access to practical applications including, for example, gas storage,[1] fluid separations,[2] catalysis,[3] sensing,[4] and even controlled drug release.[5] The literature on the topic is consequently very rich due to the immense chemical and structural possibilities as exemplified in recent review articles.[6–8] Whereas most are built up from transition metal cations, the s-block elements (and among them Li) are just gaining more attention notably because of their low weight and low toxicity.[9,10] Among the precursor organic linkers, 2,5-dihydroxyterephthalic acid‡ (DHTA or H_4-p-DHT)[11] is of special interest as it contains two sets of oxygen donors coming from both carboxylic and phenol functional groups, which may bind from one to eight metal centers depending on the protonation state (Fig. 1). When the two carboxylic groups are neutralized, the dianionic H_2-p-DHT^{2-} form can function as a bridging ligand to one (Fig. 1a), two (Fig. 1b–d), three (Fig. 1e–h), four (-Fig. 1i–m), six (Fig. 1n–o) and even seven metal centers (Fig. 1p). The negatively charged oxygen of the carboxylate group can form a chelating bond to a metal center with the adjacent phenolate oxygen, this 6 member-ring motif representing the common coordination mode for the fully deprotonated ligand.

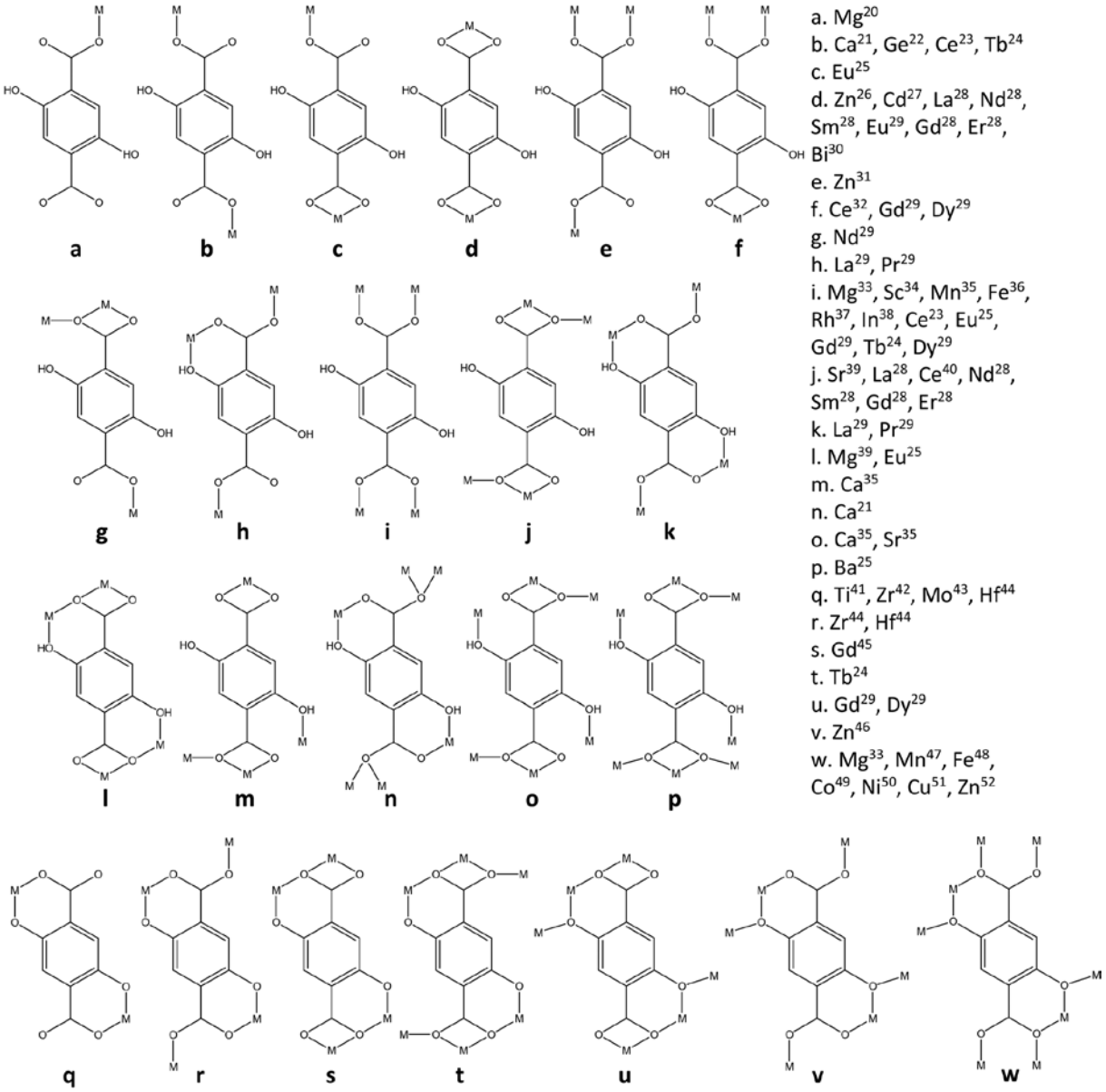

Fig. 1 The observed coordination modes reported in the literature of H_2-p-DHT^{2-} and p-DHT^{4-} bonded to di-, tri or tetravalent metal elements in coordination polymers and MOFs.[20–52]

The tetraanionic p-DHT^{4-} form can bind to two (Fig. 1q), four (Fig. 1r–s), six (Fig. 1t–v) and eight metal centers (Fig. 1w). Therefore, with its multifunctional coordination sites, the p-DHT linker can be perceived as an effective ligand in the design of various coordination compounds.

Moreover, this organic ligand is also known to be electroactive. First, in the solubilized state (non-aqueous medium) through the redox-activity of the hydroquinone moiety as reported by Savéant's group in an interesting electrochemical study performed by cyclic voltammetry focused on the coupling between electron transfer and acid–base reactions.[12] Second, in the solid state for its fully deprotonated form (p-DHT^{4-}) when combined with Li^+ or Na^+ giving rise to Li_4-p-DHT ($Li_4C_8H_2O_6$) and Na_4-p-DHT ($Na_4C_8H_2O_6$) materials, respectively, as previously demonstrated by our group[11] and Chen's group from Nankai University.[13–15] In the latter case, the p-DHT^{4-} linker appear quite promising for developing transition-metal-free electrode materials for the electrochemical energy storage. In short, p-DHT^{4-}can be reversibly oxidized in the solid state at high potential through the diphenolate ring and reduced at low potential through the carboxylate functional groups (Fig. S1,

ESI†) with concomitant insertion/removal of Li^+ (or Na^+) making the development of all-organic Li(Na)-ion batteries possible.[16] Very recently, we studied the effect of the substitution chemistry on the electrochemical properties of the Li-diphenolate moiety of p-DHT^{4-} by preparing a series of phases of general formula $M^{n+}_{2/n}(Li_2)$-p-DHT (M = Mg, Ca, and Ba) and demonstrated that substituting $MgIJLi_2$)-p-DHT ($MgLi_2C_8H_2O_6$) for Li_4-p-DHT ($Li_4C_8H_2O_6$) enables a voltage gain of +800 mV regarding the reversible delithiation/lithiation electrochemical process.[17] In other words, the $MgIJLi_2$)-p-DHT electrode material exhibits an average working potential of 3.45 V vs. Li^+/Li (against 2.55 V for Li_4-p-DHT), which places it at the level of the famous $LiFePO_4$ cathode material[18,19] while constituting a record to date in terms of lithiated organic electrode material. However, it is worth noting that in our experimental conditions the measured reversible capacity was systematically limited to half of the theoretical value[11,17] (one-electron reaction instead of the expected two-electron reaction, Fig. S1a†) probably due to the high stability of the electrogenerated radical anion in the solid state. To extent this original study on p-DHT^{4-}-based salts while mixing alkali only, we report in this paper the crystal engineering and the electrochemical behavior of Na_2IJLi_2)-p-DHT as electrode material measured in Li half-cell. This particular investigation was also the occasion to characterize the intermediate phases corresponding to the partial neutralization of 2,5-dihydroxyterephthalic acid in the Li–Na system. Thus four novel alkali metal organic frameworks (hydrates) are described with both p-DHT^{4-} and H_2-p-DHT^{2-}, namely M_2IJH_2)-p-DHT$(H_2O)_4$ (M = Li (1, 2) and Na (3)) and Na_2IJLi_2)-p-DHT$(H_2O)_8$ (4), respectively. Quite importantly, all four compounds exhibit new coordination modes of the H_2-p-DHT^{2-} or p-DHT^{4-} ligand unlisted in Fig. 1 whereas compound (4) constitutes the first example of coordination polymer combining the p-DHT^{4-} ligand with alkali metals.

2. Experimental

Chemicals and general characterization techniques

Lithium hydroxide monohydrate, lithium carbonate, sodium hydroxide monohydrate, and 2,5-dihydroxyterephthalic acid were purchased from Sigma Aldrich whereas magnesium hydroxide was obtained from Merck. The purity of these reagents were ≥98.0% and used as received. Infrared spectra were recorded using KBr pellets on a FTIR Bruker Vertex 70. Air-free pellets were prepared in glove box by mixing the sample with spectroscopic-grade potassium bromide at 1 wt%. The thermogravimetric coupled to differential scanning calorimetry (TG-DSC) experiments were performed with a SENSYSevo instrument (Setaram) using a heating rate of 5 °C min^{-1} under argon. Temperature-controlled X-ray powder diffraction (TRXRPD) patterns collected with a Bruker D8 Advance powder diffractometer equipped with an Anton Parr XRK900 high temperature chamber. Data were collected in the Bragg–Brentano geometry with a Cu-anode X-ray source operated at 40 kV and 40 mA. The Cu K_β radiation wasfiltered by means of a Ni foil. The experiments were carried out under nitrogen flow in the 5–45° 2θ range with a step of 0.016°, an acquisition time of 1.2 s per step and a heating rate of 0.1 °C s^{-1} under N_2 from 30 to 220 °C.

Protocols for crystal growth

Li_2IJH_2)-p-DHT$(H_2O)_4$ (1, form α). To a heterogeneous solution of 2,5-dihydroxyterephthalic acid (500 mg, 2.52 mmol, 1 eq.) in ultra-pure water (10 mL) using a roundbottomed flask of 25 mL was added powder of Li_2CO_3 (186.2 mg, 2.52 mmol, 1 eq.). The solution was stirred at room temperature for 18 h. The as-obtained homogenous solution was then spread in Petri dishes. After a slow evaporation

process at room temperature (24 °C), light yellow needles were formed (quantitative yield). Li_2IJH_2)-p-DHT(H_2O)$_4$ (2, form β). This polymorph has been obtained similarly except that an excess of $LiOH·H_2O$ was used in an attempt to prepare the trilithiated salt. More precisely, to a heterogeneous solution of 2,5-dihydroxyterephthalic acid (100 mg, 0.504 mmol, 1 eq.) in ultra-pure water (10 mL) was added $LiOH·H_2O$ (63.3 mg, 1.51 mmol, 3 eq.). The solution was also stirred at room temperature for 18 h. The as-obtained homogenous solution was then spread in Petri dishes. After a slow evaporation process at room temperature (24 °C), light yellow needles were formed.

Na_2IJH_2)-p-DHT(H_2O)$_4$. To a heterogeneous solution of 2,5-dihydroxyterephthalic acid (500 mg, 2.52 mmol, 1 eq.) in ultra-pure water (50 mL) was added $NaOH·H_2O$ (293 mg, 5.05 mmol, 2 eq.). The solution was stirred at room temperature for 18 h. The as-obtained homogenous solution was then spread in Petri dishes. After a slow evaporation process at room temperature (24 °C), light yellow needles were formed (quantitative yield). Na_2IJLi_2)-p-DHT(H_2O)$_8$. To degassed ultra-pure water (5 mL) using a round-bottomed flask of 25 mL were added successively in a glove box (MBRAUN, specially designed for working with moisture conditions under argon and containing less than 1 ppm of dioxygen), Na_2IJH_2)-p-DHT (300 mg, 1.24 mmol, 1 eq.) and $LiOH·H_2O$ (104 mg, 2.48 mmol, 2 eq.). The mixture was stirred at room temperature overnight. The as-obtained green homogeneous solution was then spread in Petri dishes. After a slow evaporation process under inert atmosphere (glove box) and at room temperature (24 °C), light green blocks were formed (quantitative yield). Single crystal X-ray diffraction and structure refinements

Single crystal X-ray diffraction data were collected at T = 295 K with a Bruker-Nonius Kappa CCD diffractometer using graphite monochromated Mo K_α radiation (λ = 0.71073 Å). Data for all selected crystals were corrected for absorption using JANA2006[53] within the analytical option based on the crystal morphology and optimized with X-SHAPE software.[54] The structures were solved with the ShelXT structure solution program using direct methods and refined with the ShelXL by a full-matrix least-squares technique on F_2 with WinGX interface.[55,56] All non-hydrogen atoms were refined with anisotropic thermal parameters. The hydrogen atoms bonded to carbon were refined with fixed individual displacement parameters [U_{iso}IJH) = 1.2U_{eq}IJC)], using a riding model, with C–H = 0.93 for aromatic CH. Hydrogen atoms of water molecules in all compounds and enol function in 1, 2 and 3 compounds were located in difference Fourier maps and freely refined. Crystal data, data collection and results of the final refinements for the four structures are listed in Table 1. Electrochemical testing

For the sake of comparison, the electrochemical behavior of Na_2IJLi_2)-p-DHT (anhydrous phase) was investigated in Swagelok®-type cells according to a procedure similar to the one previously reported for other DHT-based electrode materials.[11,17,57] A Li metal disc was as the negative electrode whereas the separator consisted in two fiberglass separators (Whatman®) soaked with $LiPF_6$ 1 M in ethylene carbonate/ dimethyl carbonate (EC/DMC; 1 : 1 vol/vol) as the electrolyte (LP30 from Novolyte). The composite positive electrodes were prepared in an argon-filled glovebox by simply grinding the powder of Na_2IJLi_2)-p-DHT and 33 wt% of carbon black (Ketjenblack EC-600JD, AkzoNobel) with a pestle in a mortar without binder. The cells were cycled in galvanostatic mode at 21 °C using a MPG-2 multi-channel system (Bio-Logic SAS, Seyssinet-Pariset, France) in the potential range of 2.0–3.6 V vs. Li^+/Li at a typical rate of one lithium ion exchanged per ring in 10 h.

Table 1 Crystal data, data collection and structure refinement parameters for 1, 2, 3, and 4. Pictures of single crystals are shown in supplementary
information

Compound 1, form α 2, form β 3 4
Formula $Li_2[Li_2(H_2O)_4]$-p-$DHT(H_2O)_4$ $Li_2[Li_2(H_2O)_4]$-p-$DHT(H_2O)_4$ $Na_2[Li_2]$-p-$DHT(H_2O)_8$ $Li_2[Li_2(C_8H_4O_6)(H_2O)_4]$ $Li_2[Li_2(C_8H_4O_6)(H_2O)_4]$ $Na_2[Li_2(C_8H_4O_6)(H_2O)_4]$ $Li_2Na_2[Li_2(C_8H_2O_6)(H_2O)_8]$
Crystal data
Temperature (K) 295 295 295 295
M_r 282.06 282.06 314.16 398.08
Crystal symmetry Triclinic Triclinic Triclinic Triclinic
Space group $P\bar{1}$ $P\bar{1}$ $P\bar{1}$ $P\bar{1}$
a (Å) 7.1646 (4) 7.2720 (3) 7.3226 (11) 7.3738 (11)
b (Å) 8.5039 (11) 9.1631 (3) 9.2359 (5) 7.4503 (14)
c (Å) 10.0021 (11) 10.5276 (12) 18.444 (2) 8.1802 (8)
α (deg.) 104.049 (10) 97.273 (6) 100.611 (6) 76.479 (13)
β (deg.) 97.995 (6) 110.034 (6) 90.051 (12) 66.792 (8)
γ (deg.) 96.617 (7) 111.668 (3) 101.428 (11) 84.39 (2)
V ($Å^3$) 578.34 (11) 586.18 (8) 1200.9 (2) 401.58 (11)
Z, Z′ 2, 1 2, 1 4, 2 1, 0.5
D_x (g cm^{-3}) 1.620 1.598 1.738 1.646
μ (mm^{-1}) 0.15 0.15 0.22 0.20
Crystal shape Needle Needle Needle Block
Crystal colour Light yellow Light yellow Light yellow Light green
Crystal size (mm) 0.32 × 0.07 × 0.05 0.21 × 0.14 × 0.07 0.24 × 0.22 × 0.12 0.35 × 0.31 × 0.25
Data collection
λ(Mo Kα) (Å) 0.71073 0.71073 0.71073 0.71073
Scan mode φ andω φandω φandω φand ω
θ_{min}–θ_{max} (deg.) 2.1–29.0 2.2–29.1 1.1–31.5 2.8–35.0
h, k, l ranges h = −9 → 9 h = −9 → 6 h = −10 → 10 h = −11 → 11
k = −11 → 9 k = −12 → 12 k = −13 → 13 k = −11 → 11
l = −13 → 13 l = −13 → 14 l = −27 → 27 l = −13 → 13
R_{int} 0.042 0.055 0.046 0.027
Refinement
No. of measured ref. 6884 7903 18 849 9917
No. of independent ref. 3066 3133 7947 3489
No. of ref. [I > 2σ(I)] 2175 2509 4397 2842
No. of refined parameters 222 221 442 151
Refinement method F^2 F^2 F^2 F^2
R_1 [F^2 > 2σ(F^2)] 0.048 0.046 0.056 0.036
wR (F^2) 0.118 0.128 0.159 0.092
Weighting scheme P = (F_o^2 + 2F_c^2)/3 w = 1/[$\sigma^2(F_o^2)$ + (0.0365P)^2 + 0.3655P] w = 1/[$\sigma^2(F_o^2)$ + (0.0523P)^2 + 0.2269P] w = 1/[$\sigma^2(F_o^2)$ + (0.0561P)^2 + 0.7247P] w = 1/[$\sigma^2(F_o^2)$ + (0.0314P)^2 + 0.1202P]
S 1.08 1.11 1.06 1.14
$\Delta\rho_{max}/\Delta\rho_{min}$ (e $Å^{-3}$) 0.34/−0.37 0.27/−0.38 0.44/−0.37 0.47/−0.32
Extinction coefficient
$F_c^* = kF_c[1 + 0.001 \times F_c^2\lambda^3/\sin(2\theta)]^{-1/4}$
0.023 (4

MAS-NMR investigations
The solid-state MAS-NMR spectra of all studied compounds were acquired on a Bruker Avance 500 spectrometer (B_0 = 11.8 T) using R.F. pulses at Larmor frequencies of 500 and 125.7 MHz for ^1H and ^{13}C, respectively. The samples were packed in 2.5 mm diameter zirconia rotors for $^1H \rightarrow {}^{13}C$ cross-polarization (CP) MAS-NMR and spun at 11 kHz.

3. Results and discussion

Crystal structure of $Li_2[Li_2]$-p-$DHT(H_2O)_4$ (1, form α)
Compounds 1 crystallize in the triclinic crystal system with $P\bar{1}$ space group. The asymmetric unit contains two crystallographically independent Li centers, one H_2-p-DHT^{2-} ligand and four coordinated water molecules (Fig. S2, ESI†). For each H_2-p-DHT^{2-} ligand, one bidendate carboxyl group coordinates to two Li^+ ions, the other carboxyl group

coordinates to one Li^+ ion and one hydroxyl group coordinates to one Li^+ ion, forming a new tetradentate (κ_1-κ_1)-(κ_1)-(κ_1)-μ_4 coordination mode (Fig. 2). Li(1) binds two oxygen atoms from the carboxylate groups belonging to two H_2-p-DHT^{2-} ligands and two oxygen atoms from the coordinated water molecules (Fig. 3a). The LiIJ1)–O bond distances range from 1.989(4) to 2.003(4) Å (Table S1, ESI†). Li(2) binds one oxygen atom of the carboxylate group from one H_2-p-DHT^{2-} ligand, one oxygen atom of the hydroxyl group from one H_2-p-DHT^{2-} ligand, and two oxygen atoms from the coordinated water molecules (Fig. 3a). The LiIJ2)–O bond distances range from 1.881(3) to 1.965(4) Å (Table S1†). The Li(1) and Li(2) are four-coordinated forming discrete LiO_4 tetrahedra. As shown in Fig. 3a, the discrete LiO_4 tetrahedra are bridged by the tetradentate H_2-p-DHT^{2-} ligands to generate a 2-D layer propagating along the crystallographic bc plane. The 2-D layer is further extended into a 3-D supramolecular architecture through the hydrogen-bonding interactions between the coordinated water molecule and the oxygen atom with the O···H distance varying from 1.78(4) to 2.13(3) Å (Fig. 3b, Table S2, ESI†). Topology of the underlying net is sql in standard representation of valence-bonded CPs determined using ToposPro.[58] Crystal structure of Li_2IJH_2)-p-$DHT(H_2O)_4$ (2, form β) Compound 2 is a polymorph of compound 1 and crystallizes in the triclinic crystal system with $P\bar{1}$ space group. The asymmetric unit contains two crystallographically independent Li centers, one H_2-p-DHT^{2-} ligand and four

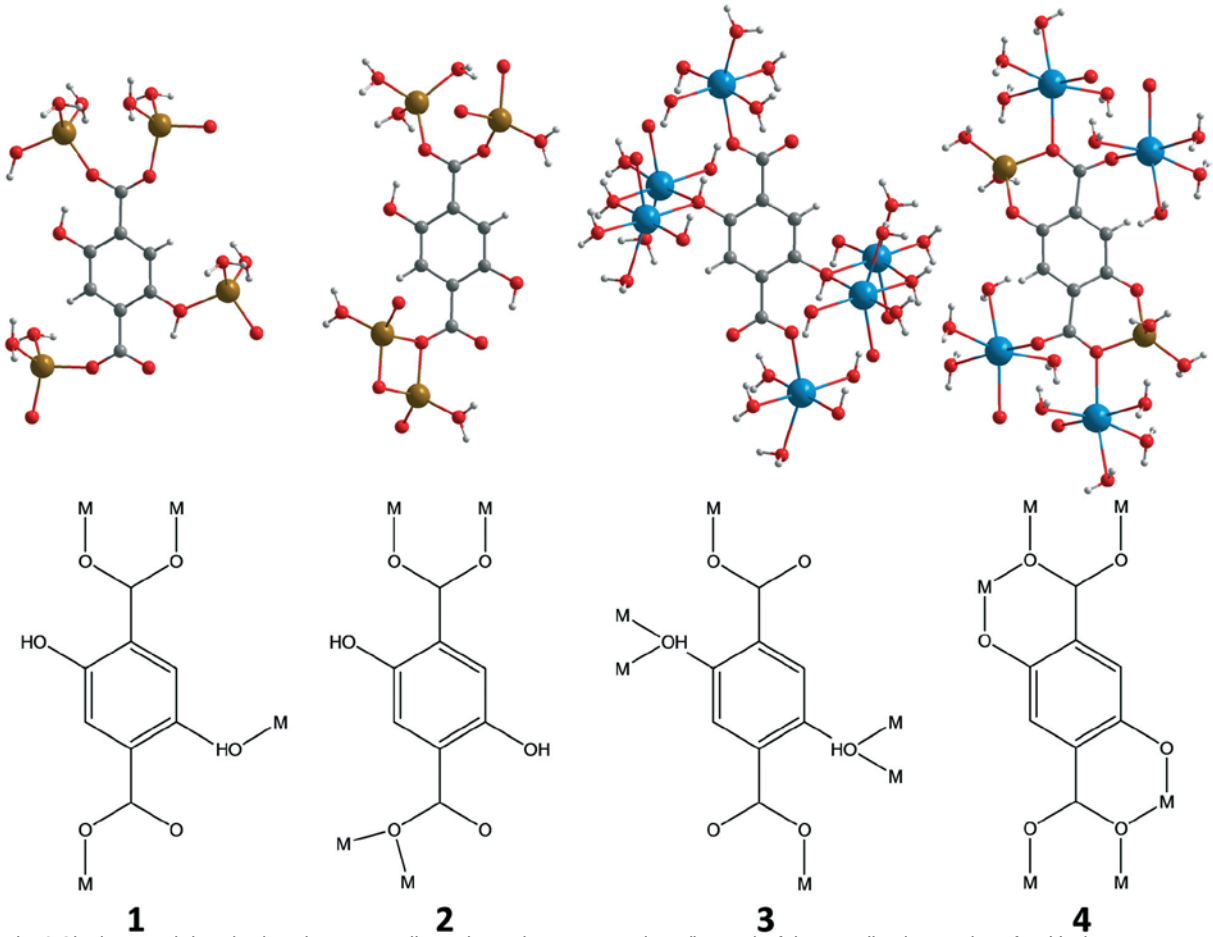

Fig. 2 Single crystal data (top) and corresponding schematic representations (bottom) of the coordination modes of M_2IJH_2)-p-$DHT(H_2O)_4$ with M
= Li (1, 2), Na (3), and Li_2Na_2-p-$DHT(H_2O)_8$ (4) compounds, respectively

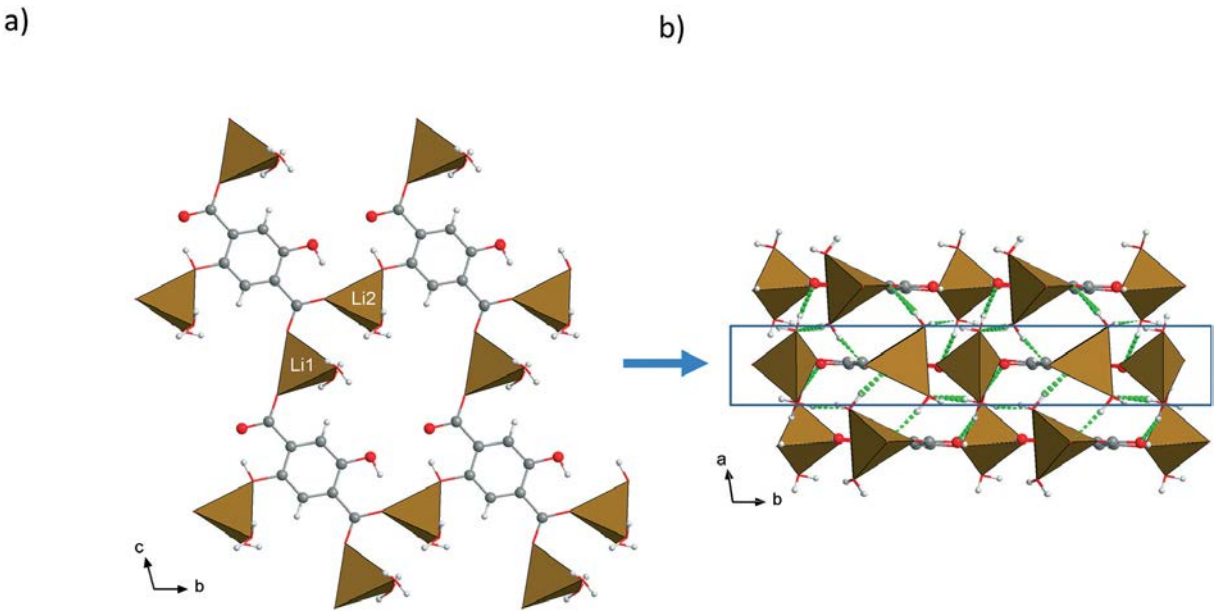

Fig. 3 2-D layer of 1 in the bc plane (a) extended to 3-D supramolecular structure through hydrogen bonds represented in green dash lines (b).

coordinated water molecules (Fig. S3, ESI†). For each H_2-p-DHT^{2-} ligand, one bidendate carboxyl group coordinates to two Li^+ ions and one monodentate carboxyl group coordinates to two Li^+ ions forming a new tetradentate (κ_1-κ_1)-(κ_1-μ_2)-μ_4 coordination mode (Fig. 2). Li(1) binds three oxygen atoms from the carboxylate groups belonging to three H_2-p-DHT^{2-} ligands and one oxygen atom from the coordinated water molecule (Fig. 4). LiIJ1)O_4 tetrahedra is quite distorted with LiIJ1)–O bond distances ranging from 1.898(3) to 2.038(3) Å and O–LiIJ1)–O bond angles varying from 91.48(11) to 118.08(15) ° (Table S1†). Li(2) binds one oxygen atom of the carboxylate group from one H_2-p-DHT^{2-} ligand and three oxygen atoms from the coordinated water molecules (Fig. 4). The LiIJ2)–O bond distances range from 1.904(3) to 1.990(3) Å
(Table S1†). The Li(1) and Li(2) are four-coordinated displaying two different inorganic motifs: one edge-sharing LiIJ1)O_4 tetrahedra forming a LiIJ1)$_2O_6$ dimer with LiIJ1)–LiIJ1) distance of 2.803(5) Å and one discrete LiIJ2)O_4 tetrahedra. The tetradentate H_2-p-DHT^{2-} ligands link Li_2O_6 dimers in the ac plane to form a 2-D layer (Fig. 4a) which is further extended into a 3-D supramolecular architecture through the hydrogenbonding interactions between the coordinated water molecule and the oxygen atom with the O···H distance ranging from 1.89(3) to 2.08(3) Å (Fig. 4b, Table S3, ESI†). Topology of the underlying net is (4,4)(0,2) in standard representation of valence-bonded CPs determined using ToposPro.[58]

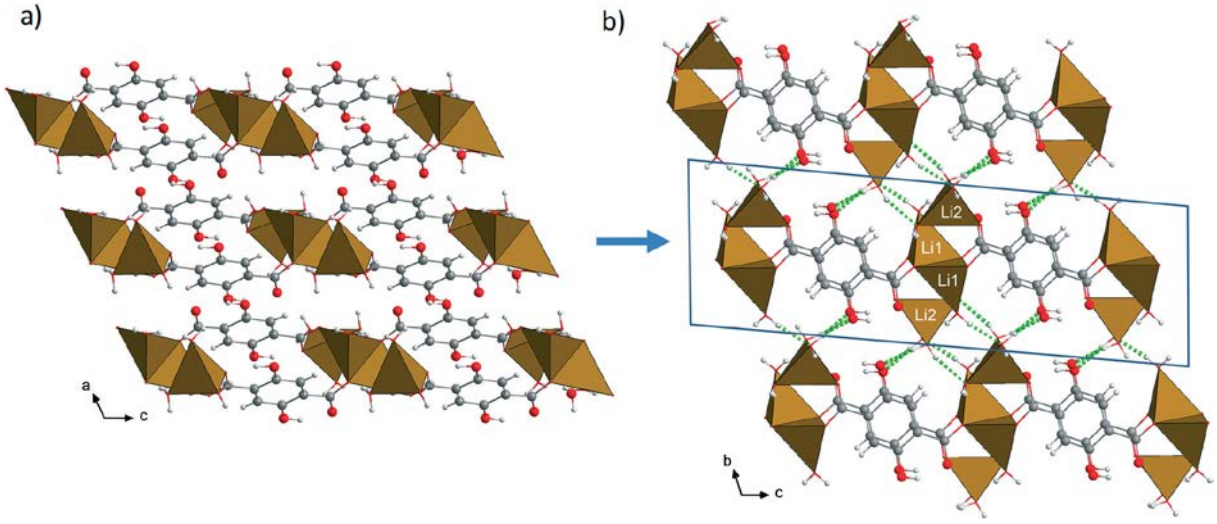

Fig. 4 2-D layer of 2 in the ac plane (a) extended to 3-D supramolecular structure through hydrogen bonds represented in green dash lines (b).

Crystal structure of Na_2IJH_2)-p-DHT(H_2O)$_4$ (3)
Compound 3 crystallizes in the triclinic crystal system with $P\bar{1}$ space group. The asymmetric unit contains four crystallographically independent Na centers, two H_2-p-DHT^{2-} ligands and eight coordinated water molecules (Fig. S4, ESI†). For each H_2-p-DHT^{2-} ligand, both monodentate carboxyl groups coordinates each to one Na^+ ion and both monodentate hydroxyl group coordinates each to two Na^+ ions forming a new hexadentate (κ_1)-(κ_1-μ_2)-(κ_1)-(κ_1-μ_2)-μ_6 coordination mode (Fig. 2). Each Na^+ ion binds two oxygen atoms from the hydroxyl groups belonging to two H_2-p-DHT^{2-} ligands, one oxygen atom of the carboxylate group from one H_2-p-DHT^{2-} ligand and three oxygen atoms from the coordinated water molecules (Fig. 5). The Na–O bond distances range from 2.3272(19) to 2.5647(18) Å (Table S1†). The sodium ions are six-coordinated forming infinite $^1_\infty[NaO_4]^{-7}$ 1-D chains of edge-sharing NaO_6 octahedra running parallel to the a axis (Fig. 5a) with Na–Na distances ranging from 3.6366(13) to 3.6883(13) Å. The edge shared between two NaO_6 octahedra is composed of one oxygen atom of the hydroxyl group from one H_2-p-DHT^{2-} ligand and one oxygen atom from the coordinated water molecule. The hexadentate H_2-p-DHT^{2-} ligands link $^1_\infty[NaO_4]^{7-}$ 1-D chains in the ab plane to form a 2-D layer (Fig. 5a) which is further extended into a 3-D supramolecular architecture through the hydrogenbonding interactions between the coordinated water molecule and the oxygen atom with the O···H distance ranging from 1.76(4) to 2.25(3) Å (Fig. 5b, Table S4, ESI†). Topology of the underlying net is 5,6L37 in standard representation of valence-bonded CPs, which is quite unusual and found in only three compounds,[59–61] determined using ToposPro.[58] Crystal structure of Na_2IJLi_2)-p-DHT(H_2O)$_8$ (4)
As previously underlined, no crystal structure constructed from the p-DHT^{4-} ligand and alkali was reported in the literature. Compound 4, which is exclusively composed of p-DHT^{4-} ligands after the deprotonation of the hydroxyl groups in H_2-p-DHT^{2-} ligands, crystallizes in the triclinic crystal system with $P\bar{1}$ space group. The asymmetric unit contains two crystallographically independent Na and Li centers, one-half of p-DHT^{4-} ligands and four coordinated water molecules (Fig. S5, ESI†). The p-DHT^{4-} ligand lies on an inversion center. For each p-DHT^{4-} ligand, both bidendate

carboxyl groups coordinates each to two Na^{+} ions and both monodentate hydroxyl group coordinates each to one Li^{+} ion forming a new hexadentate $(\kappa_1\text{-}\kappa_1)\text{-}(\kappa_2)\text{-}(\kappa_1\text{-}\kappa_1)\text{-}(\kappa_2)\text{-}\mu_6$ coordination mode wherein the carboxylate oxygen and the adjacent hydroxyl oxygen form a chelating bond to a lithium center (Fig. 2). Li^{+} ion binds one oxygen atom from the hydroxyl groups from one p-DHT^{4-} ligand, one oxygen atom of the carboxylate group from the same p-DHT^{4-} ligand and two oxygen atoms from the coordinated water molecules (Fig. 6a). The Li–O bond distances range from 1.8995(18) to 1.989(2) Å (Table S1†). Na^{+} ion binds two oxygen atoms of the carboxylate groups from two p-DHT^{4-} ligands and four oxygen atoms from the coordinated water molecules (Fig. 6a). The Na–O bond distances range from 2.3115(10) to 2.6521(10) Å (Table S1†). Li and Na atoms are respectively four and sixcoordinated and are organized into a $[Li_2Na_2O_{14}]^{24-}$ clusters of two NaO_6 octahedra and two LiO_4 tetrahedra. Both NaO_6 octahedra share an edge with Na–Na distance of 3.6855(9) Å, each LiO_4 tetrahedra sharing two corners with one oxygen atom of both NaO_6 octahedra (Fig. 6a). The hexadentate p-DHT^{4-} ligands link $[Li_2Na_2O_{14}]^{24-}$ clusters in the plane perpendicular to the ab plane to form a 2-D layer (Fig. 6a) which is further extended into a 3-D supramolecular architecture through the hydrogen-bonding interactions between the coordinated water molecule and the oxygen atom with the O···H distance ranging from 1.855(18) to 2.11(2) Å (Fig. 6b, Table S5, ESI†). Topology of the underlying net is 4,6L42 in standard representation of valence-bonded CPs determined using ToposPro.[58]

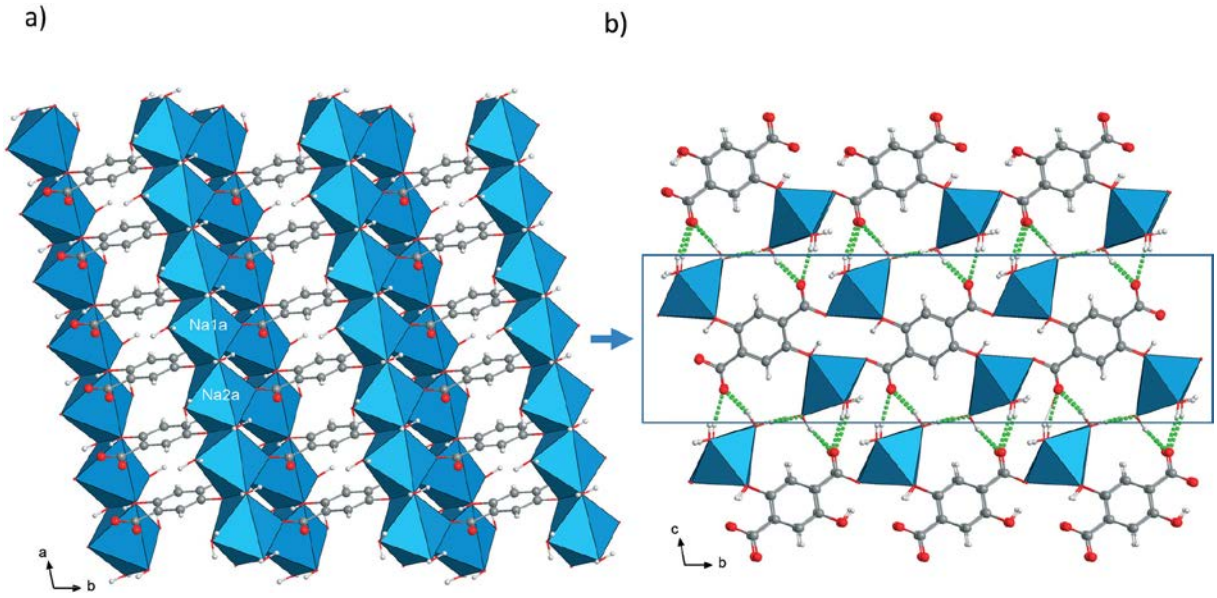

Fig. 5 2-D layer of 3 in the ab plane (a) extended to 3-D supramolecular structure through hydrogen bonds represented in green dash lines (b).

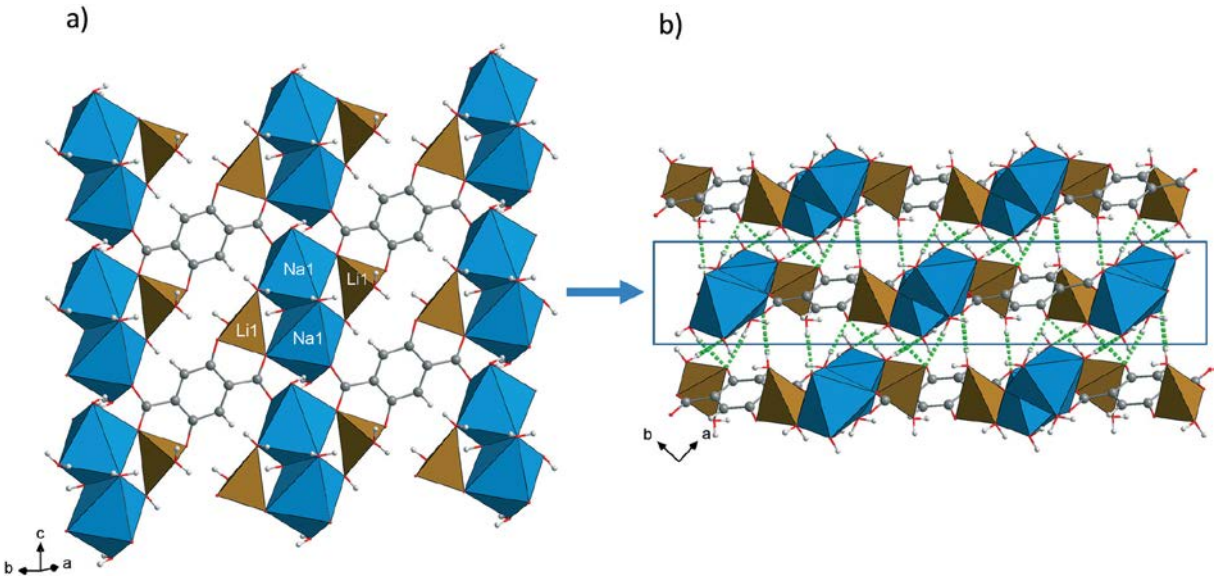

Fig. 6 2-D layer of 4 in the plane perpendicular to the ab plane (a) extended to 3-D supramolecular structure through hydrogen bonds represented in green dash lines (b).

Synthesis and electrochemical behavior of Na_2IJLi_2)-p-DHT vs. Li

Having identified a chemical way to produce pure Na_2IJLi_2)-p-DHT(H_2O)$_8$ thanks to a controlled crystal growth under inert atmosphere, the next step was to prepare the corresponding anhydrous compound in order to probe its electrochemical delithiation/lithiation behavior in Li half-cell. Thus we studied its temperature-driven evolution by both thermal analyses (TG/DSC) and temperature-controlled X-ray powder diffraction (TRXRPD) experiments under inert atmosphere (Fig. 7).

The typical thermogravimetric (TG) curve is characterized by a two successive abrupt weight losses from 85 to about 150 °C associated with two sharp endothermic phenomenon leading to an overall weight loss of ≈35% (Fig. 7a), which is consistent with the expected water loss ($\Delta m_{theo.}$ = 36.17%) to produce the corresponding anhydrous phase. The analysis of TRXRPD patterns (Fig. 7b) collected from 30 to 220 °C shows that the powder has strong preferred orientations when compared to the XRPD calculated from the single crystal refinement. This originates from the nature of the analyzed powder obtained from the crushed as-prepared single crystals. It also shows that Na_2IJLi_2)-p-DHT(H_2O)$_8$ underwent two successive phase transformations at about 80 then 100 °C in agreement with the successive steps observed by thermal analysis, which indicates that both an intermediate hydrated phase and the anhydrous Na_2IJLi_2)-p-DHT compound can be isolated. Based on the TG curve (first dehydration step, Fig. 7a), the following Na_2IJLi_2)-p-DHT(H_2O)$_{\sim 5.5}$ formula can be ascribed to this sub-hydrated phase. Note that the complete dehydration process leads to broader diffraction peaks (Fig. 7b), which can be explained by disoriented layers of the pristine 2-D structure after complete water removal and also to powder amorphization as indicated by the broad "bump" centered around 2θ = 30°. To prepare the anhydrous phase at the lab scale, a typical batch of 250 mg of Na_2IJLi_2)-p-DHT(H_2O)$_8$ (single crystals) was heated overnight at 180 °C under vacuum in a glass oven (Büchi B-585 Drying) producing yellow orange powder after the expected weight loss of ≈35%. Note that the characteristic IR vibration bands of the anhydrous Na_2IJLi_2)-p-DHT phase resemble to a certain extent to those observed with Li_4-p-DHT[11] (Fig. S7, ESI†).

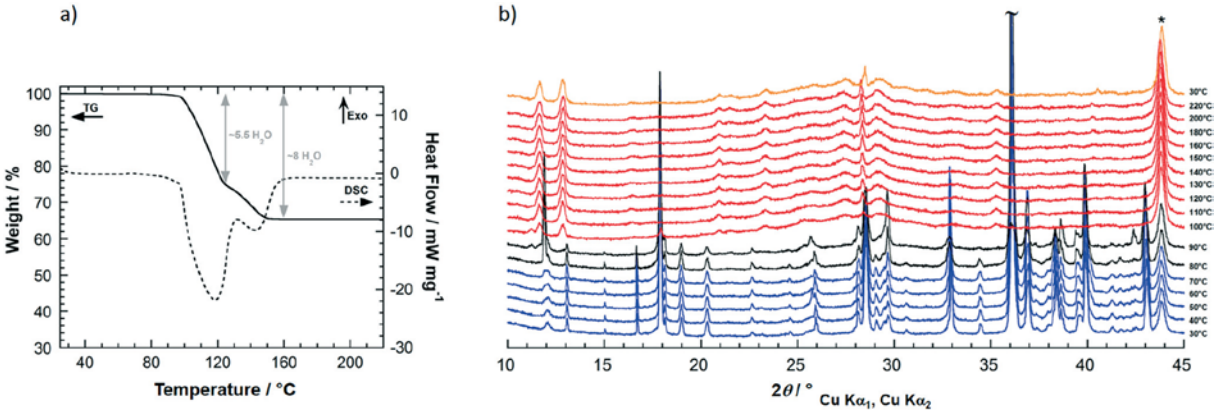

Fig. 7 a) Typical TG/DSC traces of Na_2IJLi_2)-p-DHT$(H_2O)_8$ measured under argon at a heating rate of 5 °C min^{-1}. b) TRXRPD patterns collected
from 30 to 220 °C under nitrogen flow at a heating rate of 0.1 °C s^{-1}. The last diffractogram corresponds to the anhydrous Na_2IJLi_2)-p-DHT phase
after cooling down to 30 °C (* indicates diffraction peak of the sample holder).

Since our former electrochemical studies performed on compounds of general formula $M^{n+}_{2/n}(Li_2)$-p-DHT (M = Li, Mg, Ca, and Ba) systematically demonstrated the occurrence of a reversible electrochemical delithiation/lithiation process in Li half-cell according to one-electron reaction ($\Delta x = 1$),[17] a similar reactivity was expected for M = Na at least during the first cycles because an Na/Li ion exchange reaction could occur upon cycling in the Li-cell configuration.[62] The charge/discharge electrochemical testing was performed vs. Li in Swagelok®-type cells measured in galvanostatic mode at a cycling rate of one Li^+ exchanged per Na_2IJLi_2)-p-DHT in 10 h. Fig. 8 shows the typical potential-composition trace obtained in the 2.0–3.6 V potential range vs. Li^+/Li for selected cycles to better grasp the electrochemical evolution upon cycling. Unexpectedly, a poor electrochemical behavior was immediately observed. The first cycles are characterized by (i) polarized§ and featureless charge/discharge curves, (ii) a limited number of exchanged electron/Li^+ ($\Delta x \ll 1$, Q = 74 mA h g^{-1} against 105 mA h g^{-1} expected), and (iii) a poor coulombic efficiency as shown by the progressive negative shift of the cycling curve (i.e., the capacity in charge progressively increases). After a few cycles, the cycling curve shape is substantially modified with the appearance of a reversible shoulder located at an average potential of 2.45 V vs. Li^+/Li while the coulombic efficiency is enhanced (Fig. 8, cycle #10 in black). Thereafter, the polarization effect on the charge/discharge curves is gradually mitigated giving rise to an electrochemical profile approaching that of Li_4-p-DHT[11] as demonstrated by the typical electrochemical features centered at 2.55 V vs. Li^+/Li (Fig. 8, cycle #50 in red).

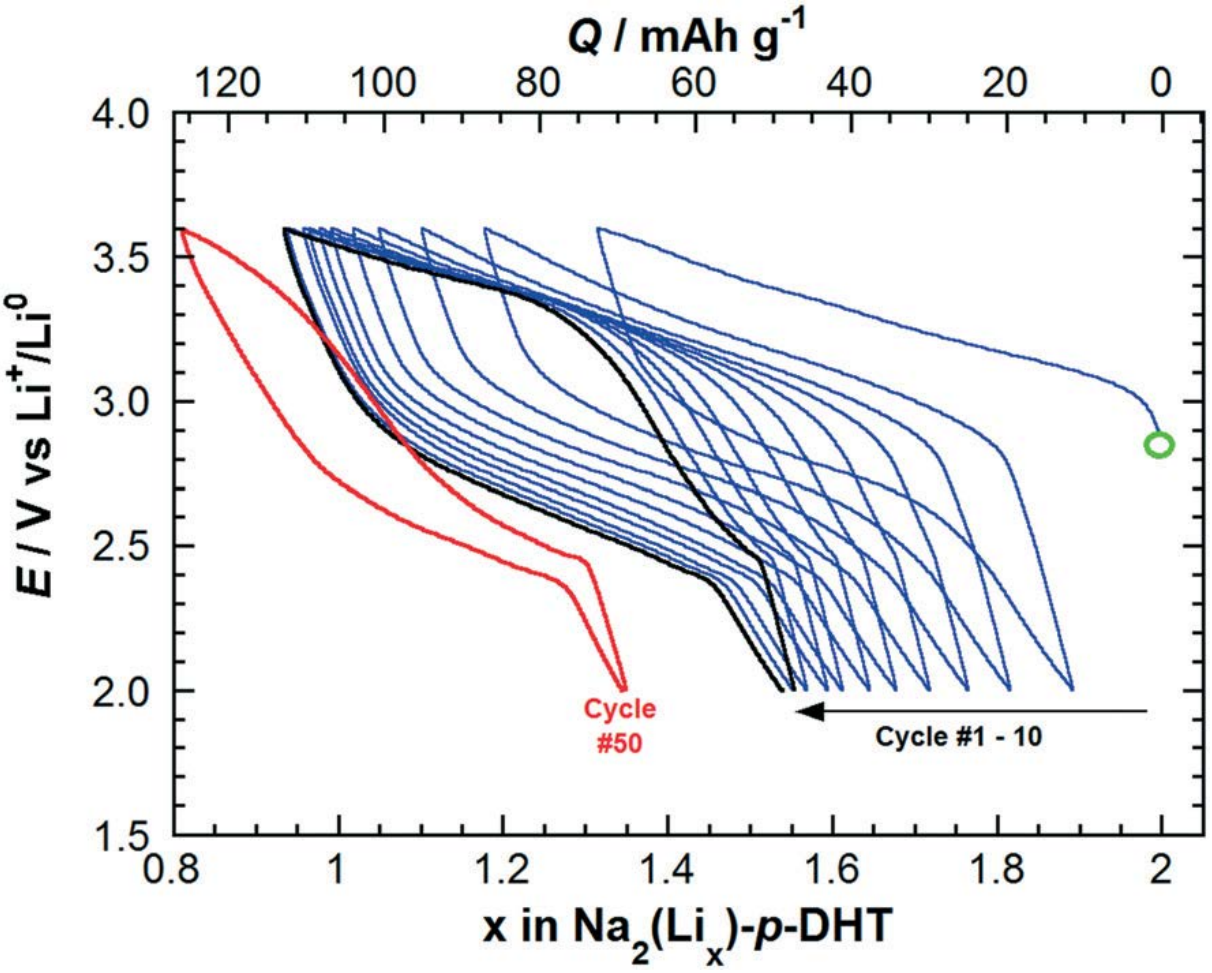

Fig. 8 Typical evolution of the galvanostatic charge/discharge curves upon cycling (selected cycles) of Na_2IJLi_2)-p-DHT measured in Li halfcell within the 2.0–3.6 V potential range at a rate of 1 Li^+ exchanged in 10 h (carbon content: 33 wt%, electrolyte: $LiPF_6$ 1 M in EC/DMC).

Although this latter behavior was expected due to the possible Na/Li ion exchange reaction in favor of lithium upon cycling, the poor cyclability observed in the first cycles was somewhat surprising but seemed to indicate an impeded electrode reaction. One possible explanation could be the occurrence of a cationic disorder between the two alkali metals in the crystal structure following the complete dehydration of Na_2IJLi_2)-p-DHT$(H_2O)_8$ inducing subsequently kinetic limitations during the delithiation/lithiation electrochemical process; it is worth remembering that similarities exist when comparing the FTIR spectra of both Na_2IJLi_2)-p-DHT phase and Li_4-p-DHT, respectively (Fig. S7, ESI†). To go further, we decided to probe in the solid state the local molecular environment of the ligand by magic-angle spinning (MAS) ^{13}C NMR. Fig. 9 displays ^{13}C CP MAS-NMR spectra of Na_2IJLi_2)-p-DHT$(H_2O)_8$ (single crystals) and the anhydrous Na_2IJLi_2)-p-DHT phase obtained after thermal annealing at 180 °C under vacuum. The spectrum obtained for the hydrated form (in black) is characterized by sharp resonances, one for each of the 4 different types of carbon nuclei present in the moiety. This feature indicates unambiguously the presence of only one well-defined single local environment for each type of carbon and allows discarding the possibility of a Li/Na exchange and any subsequent cationic disorder between the two alkali metals. This result is consistent with the refined crystal structure of (4) described above. On the other hand, the spectrum obtained in the case of the anhydrous form (in red) displays

broad and featureless resonances that are indicative of extremely disordered local environment for all the carbons of the p-DHT^{4-} ligands. The broad signals can be explained by disoriented layers of the pristine 2-D structure after complete water removal, in agreement with TRXRPD data. Nevertheless, additional chemical shifts occur, for all the resonances suggesting an additional change in the local environments of these carbons. Such a change can be due to a partial exchange between the two alkali metals in the crystal structure following the complete dehydration of Na_2IJLi_2)-p-DHT$(H_2O)_8$. Therefore, the occurrence of both signal broadening and the significant shift of the resonances support here a random exchange between Li and Na cations in the structure of the pristine dehydrated material and the as-observed electrochemical kinetic limitations.

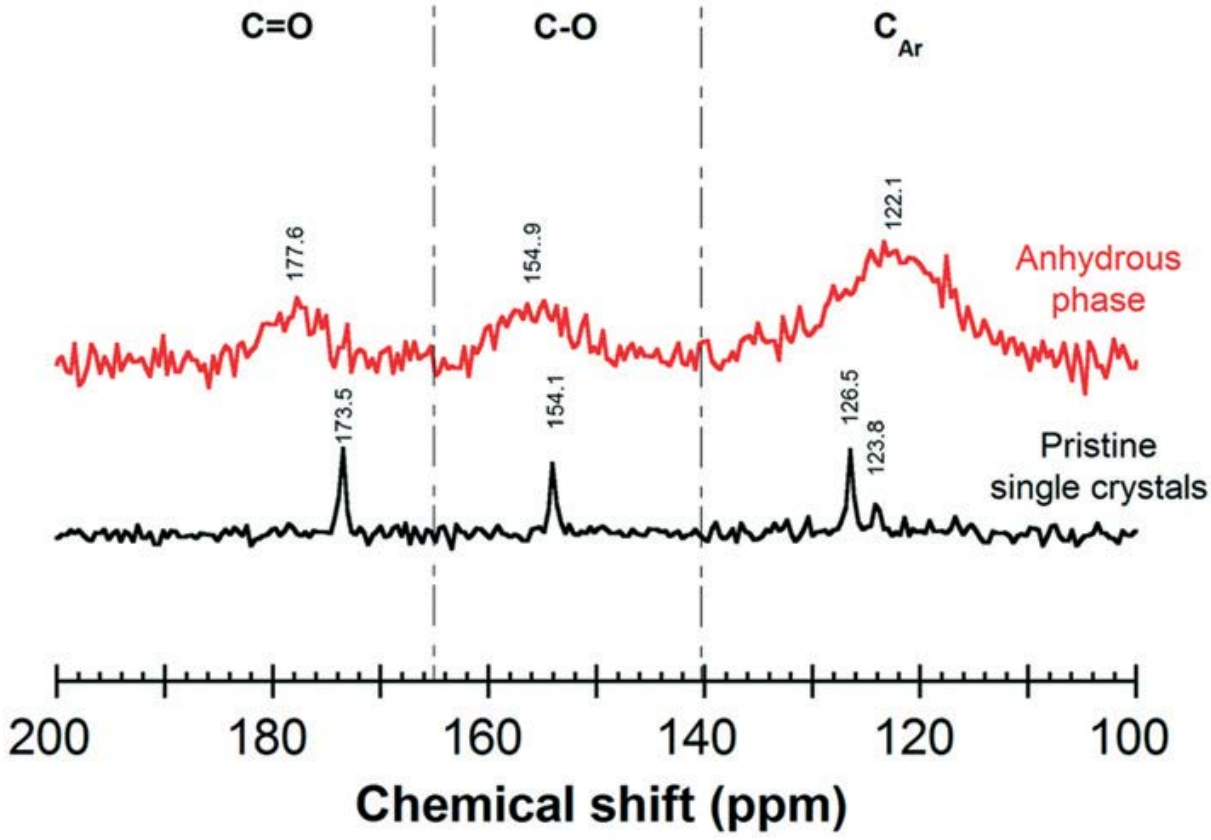

Fig. 9 Overlaid ^{13}C CP MAS-NMR spectra of Na_2lJLi_2)-p-DHT$(H_2O)_8$ (single crystals) and the anhydrous Na_2lJLi_2)-p-DHT phase obtained after thermal annealing at 180 °C under vacuum.

4. Conclusions

As part of a continuous effort to develop lithiated organic electrode materials to promote greener rechargeable Li-ion batteries, we have synthesized novel alkali salts obtained from partial to complete neutralization of 2,5-dihydroxyterephthalic acid in the Li–Na system with the aim to probe electrochemically the delithiation/lithiation process involved in Na_2lJLi_2)-p-DHT. Thus four novel alkali metal organic frameworks have been described; namely M_2lJH_2)-p-DHT$(H_2O)_4$ (M = Li (1, 2) and Na (3)) with H_2-p-DHT^{2-} ligand and Na_2lJLi_2)-p-DHT$(H_2O)_8$ (4), which constitutes the first example of coordination polymer based on the p-DHT^{4-} ligand and alkali cations. A particularly surprising result was that the poor electrochemical reversibility of Na_2lJLi_2)-p-DHT towards the delithiation/lithiation process measured in Li half-cell. Based on data recorded by ^{13}C CP MAS-NMR, it

seems that a cationic disorder between the two alkali metals occurs in the crystal structure after complete thermal dehydration of Na2lJLi2)-p-DHT(H2O)8 impeding the electrochemical deinsertion/insertion reaction as a result. Finally, it was observed a phase transformation of the pristine Na2lJLi2)-p-DHT to Li4-p-DHT upon cycling confirming the instability of sodium ions in the crystal structure.

References

1 H. Li, K. Wang, Y. Sun, C. T. Lollar, J. Li and H.-C. Zhou, Mater. Today, 2018, 21, 108–121.
2 X. Zhao, Y. Wang, D.-S. Li, X. Bu and P. Feng, Adv. Mater., 2018, 30, 1705189.
3 A. Dhakshinamoorthy, Z. Li and H. Garcia, Chem. Soc. Rev., 2018, 47, 8134–8172.
4 H. Wang, W. P. Lustig and J. Li, Chem. Soc. Rev., 2018, 47, 4729–4756.
5 G. Lan, K. Ni and W. Lin, Coord. Chem. Rev., 2019, 379, 65–81.
6 H.-C. Zhou, J. R. Long and O. M. Yaghi, Chem. Rev., 2012, 112, 673–674.
7 H.-C. J. Zhou and S. Kitagawa, Chem. Soc. Rev., 2014, 43, 5415–5418.
8 G. Maurin, C. Serre, A. Cooper and G. Férey, Chem. Soc. Rev., 2017, 46, 3104–3107.
9 D. Banerjee and J. B. Parise, Cryst. Growth Des., 2011, 11, 4704–4720.
10 A. Clough, S.-T. Zheng, X. Zhao, Q. Lin, P. Feng and X. Bu, Cryst. Growth Des., 2014, 14, 897–900.
11 S. Renault, S. Gottis, A.-L. Barrès, M. Courty, O. Chauvet, F. Dolhem and P. Poizot, Energy Environ. Sci., 2013, 6, 2124–2133.
12 C. Costentin, M. Robert and J.-M. Savéant, J. Am. Chem. Soc., 2006, 128, 8726–8727.
13 S. Wang, L. Wang, K. Zhang, Z. Zhu, Z. Tao and J. Chen, Nano Lett., 2013, 13, 4404–4409.
14 Q. Zhao, J. Wang, C. Chen, T. Ma and J. Chen, Nano Res., 2017, 10, 4245–4255.
15 S. Wang, L. Wang, Z. Zhu, Z. Hu, Q. Zhao and J. Chen, Angew. Chem., Int. Ed., 2014, 53, 5892–5896.
16 P. Poizot, F. Dolhem and J. Gaubicher, Curr. Opin. Electrochem., 2018, 9, 70–80.
17 A. Jouhara, N. Dupré, A.-C. Gaillot, D. Guyomard, F. Dolhem and P. Poizot, Nat. Commun., 2018, 9, 1–11.
18 R. Malik, A. Abdellahi and G. Ceder, J. Electrochem. Soc., 2013, 160, A3179–A3197.
19 C. Masquelier and L. Croguennec, Chem. Rev., 2013, 113, 6552–6591.
20 S. E. Henkelis, L. J. McCormick, D. B. Cordes, A. M. Z. Slawin and R. E. Morris, Inorg. Chem. Commun., 2016, 65, 21–23.
21 P.-C. Liang, H.-K. Liu, C.-T. Yeh, C.-H. Lin and V. Zima, Cryst. Growth Des., 2011, 11, 699–708.
22 X. Wang, X. Shen, Y.-J. Zhang, F. Su, G. Liu, Y. Xu and D.-R. Zhu, Inorg. Chem. Commun., 2013, 35, 45–49.
23 L.-T. Zhao, Y.-N. Wei, C.-B. Li, X.-S. Song and J.-R. Li, Z. Kristallogr. - New Cryst. Struct., 2017, 232, 241–243.
24 S. L. Anderson, A. Gładysiak, P. G. Boyd, C. P. Ireland, P. Miéville, D. Tiana, B. Vlaisavljevich, P. Schouwink, W. van Beek, K. J. Gagnon, B. Smit and K. C. Stylianou, CrystEngComm, 2017, 19, 3407–3413.
25 Z.-P. Wang, B. Hu, X.-H. Qi, N.-N. Shen and X.-Y. Huang, Dalton Trans., 2016, 45, 8745–8752.
26 N. E. Ghermani, G. Morgant, J. d'Angelo, D. Desmaële, B. Fraisse, F. Bonhomme, E. Dichi and M. Sgahier, Polyhedron,

2007, 26, 2880–2884.
27 L. Xue, Z. Kristallogr. - New Cryst. Struct., 2018, 233, 271–272.
28 Y.-L. Wang, Y.-L. Jiang, Q.-Y. Liu, Y.-X. Tan, J.-J. Wei and J. Zhang, CrystEngComm, 2011, 13, 4981–4987.
29 Y.-L. Wang, Y.-L. Jiang, Z.-J. Xiahou, J.-H. Fu and Q.-Y. Liu, Dalton Trans., 2012, 41, 11428–11437.
30 A. D. Burrows, M. Jurcic, M. F. Mahon, S. Pierrat, G. W. Roffe, H. J. Windle and J. Spencer, Dalton Trans., 2015, 44, 13814–13817.
31 T. Yamada and H. Kitagawa, J. Am. Chem. Soc., 2009, 131, 6312–6313.
32 L. Xue, S. Han-Yang, H. Shuang, W. Jia-Jun, M. Hao-Yan, L. Chun-Ling, Z. Shou-Cai and L. Chuan-Bi, Z. Kristallogr. - New Cryst. Struct., 2019, 234, 259–260.
33 P. D. C. Dietzel, R. Blom and H. Fjellvåg, Eur. J. Inorg. Chem., 2008, 2008, 3624–3632.
34 P. D. C. Dietzel, R. Blom and H. Fjellvåg, Dalton Trans., 2006, 2055–2057.
35 P. C. Dietzel, R. Blom and H. Fjellvåg, Z. Anorg. Allg. Chem., 2009, 635, 1953–1958.
36 T. Devic, P. Horcajada, C. Serre, F. Salles, G. Maurin, B. Moulin, D. Heurtaux, G. Clet, A. Vimont, J.-M. Grenèche, B. L. Ouay, F. Moreau, E. Magnier, Y. Filinchuk, J. Marrot, J.-C. Lavalley, M. Daturi and G. Férey, J. Am. Chem. Soc., 2010, 132, 1127–1136.
37 J. F. Bickley, R. P. Bonar-Law, C. Femoni, E. J. MacLean, A. Steiner and S. J. Teat, J. Chem. Soc., Dalton Trans., 2000, 4025–4027.
38 X. Zhao, X. Bu, E. T. Nguyen, Q.-G. Zhai, C. Mao and P. Feng, J. Am. Chem. Soc., 2016, 138, 15102–15105.
39 A. Douvali, G. S. Papaefstathiou, M. P. Gullo, A. Barbieri, A. C. Tsipis, C. D. Malliakas, M. G. Kanatzidis, I. Papadas, G. S. Armatas, A. G. Hatzidimitriou, T. Lazarides and M. J. Manos, Inorg. Chem., 2015, 54, 5813–5826.
40 S. Nayak, H. P. Nayek, C. Pietzonka, G. Novitchi and S. Dehnen, J. Mol. Struct., 2011, 1004, 82–87.
41 H. Assi, L. C. Pardo Pérez, G. Mouchaham, F. Ragon, M. Nasalevich, N. Guillou, C. Martineau, H. Chevreau, F. Kapteijn, J. Gascon, P. Fertey, E. Elkaim, C. Serre and T. Devic, Inorg. Chem., 2016, 55, 7192–7199.
42 M. Maercz, D. S. Wragg, P. D. C. Dietzel and H. Fjellvåg, Acta Crystallogr., Sect. E: Struct. Rep. Online, 2013, 69, m153.
43 Z. Ji, C. Trickett, X. Pei and O. M. Yaghi, J. Am. Chem. Soc., 2018, 140, 13618–13622.
44 H. Chun and D. Moon, Cryst. Growth Des., 2017, 17, 2140–2146.
45 K. L. Gurunatha, S. Mohapatra, P. A. Suchetan and T. K. Maji, Cryst. Growth Des., 2009, 9, 3844–3847.
46 F. Luo, C. Yan, L. Dang, R. Krishna, W. Zhou, H. Wu, X. Dong, Y. Han, T.-L. Hu, M. O'Keeffe, L. Wang, M. Luo, R.-B. Lin and B. Chen, J. Am. Chem. Soc., 2016, 138, 5678–5684.
47 Q. Gao, F.-L. Jiang, M.-Y. Wu, Y.-G. Huang, W. Wei, Q.-F. Zhang and M.-C. Hong, Aust. J. Chem., 2010, 63, 286–292.
48 D. J. Xiao, E. D. Bloch, J. A. Mason, W. L. Queen, M. R. Hudson, N. Planas, J. Borycz, A. L. Dzubak, P. Verma, K. Lee, F. Bonino, V. Crocellà, J. Yano, S. Bordiga, D. G. Truhlar, L. Gagliardi, C. M. Brown and J. R. Long, Nat. Chem., 2014, 6, 590–595.
49 P. D. C. Dietzel, Y. Morita, R. Blom and H. Fjellvåg, Angew. Chem., Int. Ed., 2005, 44, 6354–6358.
50 P. D. C. Dietzel, B. Panella, M. Hirscher, R. Blom and H. Fjellvåg, Chem. Commun., 2006, 959–961.
51 W. L. Queen, M. R. Hudson, E. D. Bloch, J. A. Mason, M. I. Gonzalez, J. S. Lee, D. Gygi, J. D. Howe, K. Lee, T. A. Darwish, M. James, V. K. Peterson, S. J. Teat, B. Smit, J. B. Neaton, J. R. Long and C. M. Brown, Chem. Sci., 2014, 5, 4569–4581.
52 P. D. C. Dietzel, R. E. Johnsen, R. Blom and H. Fjellvåg,

Chem. – Eur. J., 2008, 14, 2389–2397.
53 V. Petříček, M. Dušek and L. Palatinus, Z. Kristallogr. - Cryst. Mater., 2014, 229, 345–352.
54 Stoe & Cie, X-SHAPE, Stoe & Cie, Darmstadt, Germany, 1998.
55 G. M. Sheldrick, Acta Crystallogr., Sect. A: Found. Adv., 2015, 71, 3–8.
56 L. J. Farrugia, J. Appl. Crystallogr., 2012, 45, 849–854.
57 S. Gottis, A.-L. Barrès, F. Dolhem and P. Poizot, ACS Appl. Mater. Interfaces, 2014, 6, 10870–10876.
58 V. A. Blatov, A. P. Shevchenko and D. M. Proserpio, Cryst. Growth Des., 2014, 14, 3576–3586.
59 J.-F. Petit, A. Gleizes and J.-C. Trombe, Inorg. Chim. Acta, 1990, 167, 51–68.
60 M. Arıcı, O. Z. Yeşilel and M. Taş, J. Solid State Chem., 2017, 245, 146–151.
61 J.-J. Wang, L. Tang, M.-L. Zhang, L.-J. Gao, Y.-X. Ren, X.-Y. Hou and F. Fu, J. Mol. Struct., 2015, 1085, 215–221.
62 E. Deunf, N. Dupré, E. Quarez, P. Soudan, D. Guyomard, F. Dolhem and P. Poizot, CrystEngComm, 2016, 18, 6076–6082.